analytical chemistry

pubs.acs.org/ac Article

Simultaneous Detection of Bladder Cancer Exosomal MicroRNAs Based on Inorganic Nanoflare and DNAzyme Walker

Xiao Zhang,[‖] Xiaowei Wei,[‖] Jijin Qi, Jie Shen, Junwen Xu, Guangyu Gong, Yong Wei, Jian Yang, Qingyi Zhu, Tingting Bai, Zhirui Guo, Xiaojun Qu,* and Yefei Zhu*

Cite This: *Anal. Chem.* 2022, 94, 4787−4793 Read Online

ACCESS | Metrics & More | Article Recommendations | Supporting Information

ABSTRACT: Bladder cancer (BC) is one of the most common cancers in the world, with high morbidity and mortality. It is essential to develop a non-invasive, highly accurate, and simple method for BC diagnosis. This work proposed a fluorescent biosensor based on inorganic nanoflares combined with a DNAzyme walker for the simultaneous detection of BC exosomal microRNAs (miRNAs). This biosensor was constructed on the Au nanoparticle (AuNP) modified with the carbon dot (CD)-labeled substrates and DNAzyme strands (AuNP@CDs inorganic nanoflares-DNAzyme, APCD). In the presence of target miRNAs, DNAzyme was activated and then cleaved the CD-labeled substrates and automatically walked along the AuNP, allowing fluorescence recovery. Due to the structure and functional composition, the APCD biosensors demonstrated high sensitivity and specificity, with the reached limit of detection for a single miRNA at the femtomolar level and wide linear range from 50 fM to 10 nM. Furthermore, the simultaneous analysis of BC-related exosomal miR-133b and miR-135b in clinical serum specimens was achieved and consistent with qRT-PCR, suggesting it is a potential method for the diagnosis of BC and other cancers.

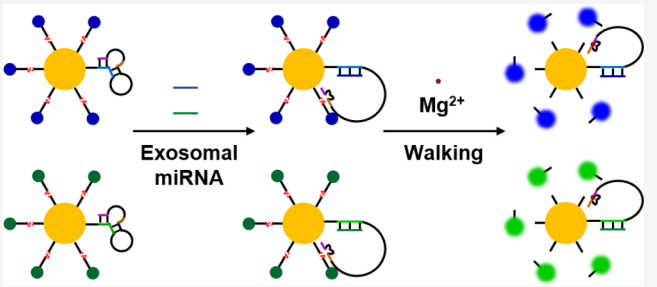

Bladder cancer (BC) is one of the most common malignant diseases of the genitourinary system. The poor prognosis of this disease arises partly from the lack of effective means of early diagnosis.[1,2] Cystoscopy and urine cytology are still the gold standards for the diagnosis and prognosis monitoring of BC. However, cystoscopy is invasive, while urine cytology has less sensitivity.[3] Therefore, the development of a novel non-invasive, highly sensitive, and specific strategy for the diagnosis of BC is of great significance. Exosomes are extracellular vesicles with a diameter from 30 to 200 nm, containing proteins, lipids, microRNAs (miRNAs), and other RNA species.[4−6] Accumulating studies indicated that exosomal miRNAs play a key role in regulating cancer progression,[7] which have thus been evaluated as reliable biomarkers for non-invasive detection of cancers.[8,9] However, the conventional detection methods of exosomal miRNAs generally require complicated, expensive, and professional operation, which makes analysis of the miRNA a big challenge. In addition, the low expression abundance of the exosomal miRNA poses the direct technical problem to quantitative detection. Therefore, it is extremely urgent to develop a sensitive, specific, and simple strategy for exosomal miRNA detection.

Benefiting from the fast sensing and direct signal output,[10] a nanoflare sensor has potential in being applied for miRNA detection.[11−14] Liu et al. utilized gold nanoflares in miRNA detection, and the limit of detection (LOD) ∼300 pM was obtained.[12] However, the conventional organic dye-labeled nanoflares have limitations of photostability and sensitivity.

As a kind of inorganic material with high fluorescence brightness and photostability,[15] carbon dots (CDs) have the advantages of simple preparation and simultaneous excitation, which can remedy for the poor photostability of nanoflares.[16−18] If combined with some signal amplification strategy, it is beneficial to improve the sensitivity of quantitative analysis of the miRNA. DNAzyme is a catalytic functional oligonucleotide with inherent characteristics of self-directed movement and integration of repetitive stepping,[19,20] which makes it an ideal signal amplifier.[21−23] However, the construction and signal system of CD-based material still need to be further optimized for high-sensitivity quantitative analysis of miRNAs.

In this work, we proposed a fluorescent biosensor based on inorganic nanoflares combined with a DNAzyme walker for the simultaneous detection of BC-related exosomal miRNAs. As shown in Scheme 1, the nanoflare was composed of a Au

Received: December 27, 2021
Accepted: March 3, 2022
Published: March 11, 2022

https://doi.org/10.1021/acs.analchem.1c05588
Anal. Chem. 2022, 94, 4787−4793

Scheme 1. Schematic Illustration of the APCD Biosensors for Simultaneous Detection of Exosomal miRNAs

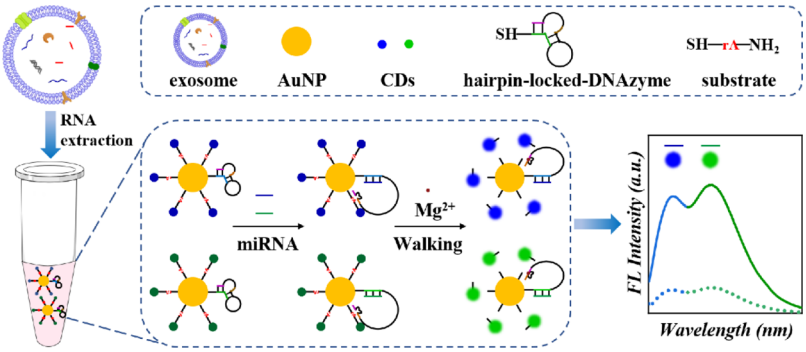

nanoparticle (AuNP) core coated with a high-density shell of CD-labeled substrates. Meanwhile, the DNAzyme strands were integrated onto the AuNP surface, and an exquisite AuNP@CD inorganic nanoflare-DNAzyme (APCD) biosensor was constructed. In the absence of the target miRNA, the DNAzyme was inactive owing to its hairpin structure, while the fluorescence of CDs was quenched by the AuNP. Conversely, the presence of the target miRNA could unlock the DNAzyme hairpin that can be hybridized with the substrate. Then, the substrate was cleaved by the DNAzyme in coordination with Mg^{2+}, resulting in the release of CDs and fluorescence recovery. DNAzyme walking was achieved by programmatically initiating subsequent substrate reactions. In this process, a trace amount of target miRNAs could cause the cleavage of abundant CD-labeled substrates from the AuNP surface to present an amplified fluorescence signal. Simultaneous analysis of two kinds of exosomal miRNAs was performed by substrate modification of blue-emitting CDs (bCDs) and green-emitting CDs (gCDs), respectively. The results indicated that APCD biosensors could quantitatively detect exosomal miRNAs within a linear range from 50 fM to 10 nM. In addition, the system had excellent analytical performance in the detection of BC-related exosomal miRNAs in the clinical serum specimen. Therefore, the APCD biosensors may have an ideal application prospect in exosomal miRNAs-based BC diagnosis.

EXPERIMENTAL SECTION

Materials. Tris (2-carboxyethyl) phosphine hydrochloride (TCEP), 1-ethyl-3-(3-dimethyllaminopropyl) carbodiimide hydrochloride (EDC), and *N*-hydroxy succinimide (NHS) were purchased from Sigma-Aldrich. The CD63 antibody and CD81 antibody were purchased from Santa Cruz (CA, USA). Goat anti-mouse IgG was purchased from KeyGEN (Nanjing, China). Total Exosome Isolation Reagent and TRIzol Reagent were purchased from Invitrogen (CA, USA). The miRNA 1st-Strand cDNA Synthesis Kit and miRNA Universal SYBR qPCR Master Mix were purchased from Vazyme (Nanjing, China). All oligonucleotides were synthesized by GenScript (Nanjing, China) and are listed in Table S1. Six paired serum samples from BC patients and normal controls (NC) were collected from the Second Affiliated Hospital of Nanjing Medical University and Jiangsu Province Hospital of Chinese Medicine according to the guidelines issued by the ethics committee.

Instruments. A RF-6000 fluorescence spectrophotometer (Shimadzu, Japan) was utilized to test fluorescence spectra. A UV-3600 spectrophotometer (Shimadzu, Japan) was applied to record UV−vis spectra. A JEM-2100 transmission electron microscopy microscope (TEM) (JEOL, Japan) was used to image the morphology of nanoparticles. Fourier transform infrared (FTIR) was measured on the Nicolet 5700 FTIR spectrometer (Thermo Fisher, USA). Quantitative real-time PCR (qRT-PCR) was performed on the StepOnePlus Real-Time PCR system (ABI, USA). Nanoparticle tracking analysis (NTA) was carried out with the ZetaView (PMX, Germany). Dynamic light scattering (DLS) was observed by using a Zetasizer Nano ZS90 (MALVERN, UK).

Preparation of CDs and AuNPs. In this work, bCDs and gCDs were prepared by microwave treatment of citric acid and urea, respectively.[24,25] The synthesis of AuNPs (17 nm in diameter) was performed by a sodium citrate reduction method.[26]

Synthesis of DNA (DNAzyme and Substrate)-Functionalized AuNPs. The AuNPs-DNA was synthesized according to the established procedure.[27] First, the DNAzyme sequences were annealed at 95 °C for 2 min and then slowly cooled to room temperature to obtain the hairpin-locked DNAzyme. Subsequently, the thiolated DNAzyme (1 μM, 20 μL) and substrates (1 μM, 80 μL) were treated with TCEP (2.5 μM, 100 μL) for 1 h, and then, 150 μL of AuNPs was added and incubated overnight. SDS (1%, 4 μL) was mixed with the above-mentioned solution for 30 min, and then, NaCl (2 M) was added every 0.5 h until the final concentration reached 0.7 M. Over another 24 h, the solution was centrifuged at 13,000 rpm for 20 min and washed with deionized water three times and then resuspended in 100 μL of Tris-HCl (10 mM, pH 7.4).

Synthesis of APCD Biosensors. EDC and NHS (0.02 M final concentration) were added into the CD solution (10 μL) and oscillated for 30 min. Then, AuNPs-DNA solution was added into the activated CD solution and kept reacting for 4 h. The APCD was centrifugally (13,000 rpm, 20 min) collected and dispersed in 100 μL of Tris-HCl (10 mM, pH 7.4) for further use.

Polyacrylamide Gel Electrophoresis (PAGE). The samples consisting of the DNAzyme (2 μM, 12 μL), target miRNA (2 μM, 12 μL), substrate (2 μM, 3 μL), and Mg^{2+} (5 mM, 3.5 μL) were incubated at 37 °C for 3 h. Non-denaturing polyacrylamide gel (20%) was used to analyze the products. Electrophoresis was performed at a constant potential of 90 V for 120 min with loading of each sample (10 μL) into the lanes. GelRed was used as the fluorescent duplex intercalator and then imaged by using the gel imaging system.

Fluorescence Detection. In sensitivity analysis, miRNAs with the increasing concentrations (0 fM, 10 fM, 50 fM, 100

https://doi.org/10.1021/acs.analchem.1c05588
Anal. Chem. 2022, 94, 4787−4793

fM, 1 pM, 10 pM, 100 pM, 1 nM, 10 nM, and 100 nM) were incubated in APCD solution (37 °C, 3 h), and the fluorescence spectra were measured with excitation at 380 nm. For specificity evaluation, the target miRNA and point-mutation sequences (1-mut, 3-mut, and 5-mut) and random miRNA sequences (1 nM) were added into the APCD solution for fluorescence intensity detection. In the simultaneous analysis of miRNAs, different combiniations of two target miRNAs (miR-135b, miR133b, and miR-135b+miR-133b) were incubated with the mixture of two colors of APCD, respectively. The detection signal intensity was reflected by measuring the fluorescence spectrum.

Exosomal RNA Isolation and qRT-PCR. Based on the previous work of our research group, we analyzed the BC-related exosomal miRNAs for diagnosis.[28,29] Here, we validated the expression of two kinds of miRNAs (miR-133b and miR-135b) in BC and NC serum exosomes, respectively. According to the manufacturer's specifications, exosomes were isolated from serum using the Total Exosome Isolation and then identified by TEM, a western blot, and NTA. The exosomal RNA was extracted by the TRIzol Reagent. The cDNA was synthesized using the miRNA 1st Strand cDNA Synthesis Kit. The qRT-PCR was performed using the miRNA Universal SYBR qPCR Master Mix. Cel-miR-39-3p was used as the external control. The relative expression of the exosomal miRNA was calculated by the $2^{-\triangle\triangle CT}$ method.

RESULTS AND DISCUSSION

Characterization of Exosomes. According to International Society for Extracellular Vesicles 2018 (ISEV 2018) guidelines, the exosomes extracted were characterized by the morphology, characteristic proteins, and particle size distribution. As shown in Figure 1a, the exosome displayed a saucer-like membrane structure. Western blot (WB) experiments confirmed the presence of characteristic protein markers CD63 and CD81 on the exosome membrane, corresponding to the 22 and 26 kDa bands, respectively (Figure 1b). NTA calculated the exosomes with a total particle concentration of 9.8×10^{10} particles/mL. It showed that about 98% of extracellular vesicles were within the size of 0−200 nm with a mean diameter of 97.8 nm (Figure 1c). These characteristics proved the effective extraction of exosomes from serum specimens.

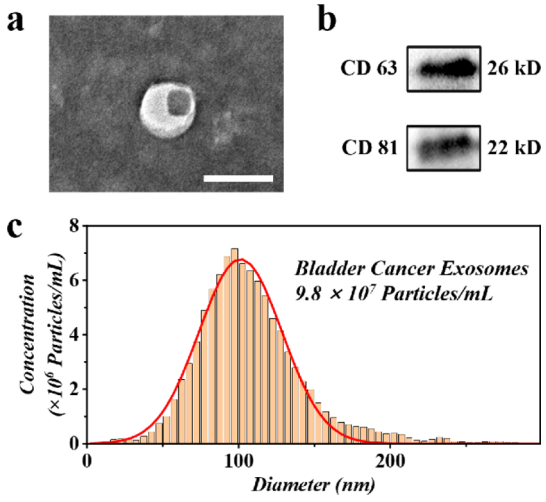

Figure 1. Characterization of extracted exosomes from serum specimens. (a) TEM image of exosomes. The scale bar is 100 nm. (b) Western blot bands of CD63 and CD81 on the exosome vesicle membrane. (c) NTA of 1000× diluted exosomes.

qRT-PCR Analysis of Exosomal miRNAs. qRT-PCR was used to analyze the expression of BC-related exosomal miRNAs in the serum specimens for target validation. As shown in Figure S1, compared with the NC group, the expression of miR-135b in the BC serum-derived exosomes was increased while that of miR-133b was decreased. Notably, miR-133b was significantly correlated with the progression of BC.[30] Hence, the detection of the two candidate exosomal miRNAs may be of great significance in the diagnosis of BC.

Characterization of APCD Biosensor. The morphology of CDs was characterized by TEM. As shown in Figure S2a,b, the CDs were spherical and monodispersed, with sizes of ∼2.4 nm (bCDs) and 3 nm (gCDs). Fluorescence emission spectra and UV−vis absorption spectra of bCDs and gCDs are displayed in Figure S2c,d. Under 380 nm excitation, the maximum emission spectra of the two kinds of CDs were 440 and 537 nm, respectively. The UV−vis absorption spectrum displayed a peak at 333 nm which originated from n−π^* transition of C═O. Furthermore, the surface functional groups of the carboxylated CDs were detected by FTIR (Figure S2e). Under continuous irradiation, the fluorescence intensity of CDs did not change significantly (Figure S2f), indicating that the CDs have excellent photostability.

The AuNP was modified with the DNAzymes and substrates by the Au−S bond (AuNPs-DNA), and then, carboxylated CDs were conjugated to the amino terminus of the substrate, and thus, the AuNP@CD inorganic nanoflare-DNAzyme (APCD) biosensor was constructed. The synthetic AuNPs were uniform with an average size of 17 nm (Figure 2a). After the surface conjugation, multiple CDs were assembled on the surface of AuNPs (Figure 2b). DLS showed that the AuNPs, AuNPs-DNA, and APCD had the average sizes of 19, 38, and 56 nm, respectively, which indicated the assembly of DNA and CDs (Figure 2c). The UV−vis absorption spectra (Figure 2d) indicated that the maximum extinction of AuNPs was 520 nm.

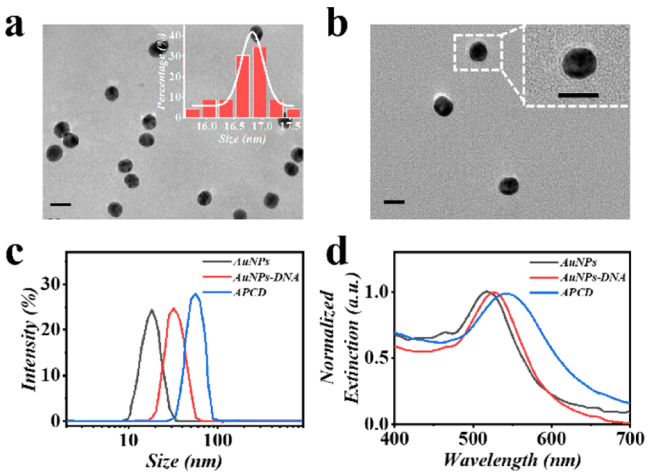

Figure 2. Characterization of the synthetic the AuNPs, AuNPs-DNA, and APCD biosensor. (a) TEM image of AuNPs and the size distribution plot. The scale bar is 20 nm. (b) TEM images of the APCD biosensor. Scale bars are 20 nm. (c) DLS measurement of AuNPs, AuNPs-DNA, and APCD. (d) UV−vis spectra of AuNPs, AuNPs-DNA, and APCD.

https://doi.org/10.1021/acs.analchem.1c05588
Anal. Chem. 2022, 94, 4787−4793

The modification of DNA molecules resulted in a spectral red shift to 525 nm. After the second layer assembly of CDs, the spectral peak shifted to 542 nm. These characterizations indicated the efficient construction of the APCD.

Feasibility of DNAzyme as Signal Amplifier. The DNAzyme strand was a monomolecular structure consisting of a DNAzyme sequence and a target miRNA recognition sequence (green color). The DNAzyme sequence is composed of a catalytic core flanked by two binding arms (brown and purple color). After the thermal denaturation and annealing, the hairpin structure was obtained (Figure 3a). The DNAzyme

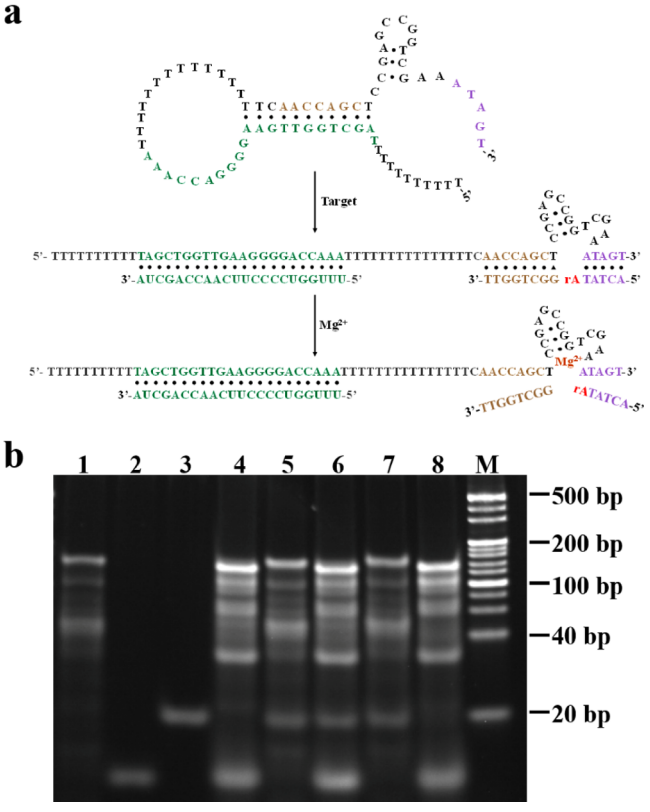

Figure 3. Analysis of the target-triggered DNAzyme walking process by non-denaturing PAGE. (a) Schematic diagram of hairpin-locked -DNAzyme and its walking principle. (b) Lane 1, hairpin-locked DNAzyme (D); lane 2, target miRNA (T); lane 3, substrate (S); lane 4, D + T; lane 5, D + S; lane 6, D + T + S; lane 7, D + S + Mg^{2+}; lane 8, D + T + S + Mg^{2+}; and M, 20−500 bp DNA ladder.

was inactive as it was integrated into the hairpin structure. When the target miRNA was recognized, the hairpin structure was opened, and the DNAzyme was released. Then, the binding arms of DNAzyme were hybridized with substrates, and the rA linkage was cleaved with the assistance of Mg^{2+}. Therefore, the hairpin-locked DNAzyme could only be opened by the target, offering an ideal specificity for miRNA detection.

The target-triggered DNAzyme walking process was analyzed by non-denaturing PAGE (Figure 3b). Here, three oligonucleotide sequences were involved, including the hairpin-locked DNAzyme (D), target miRNA (T), and substrate (S), which corresponded to lane 1, lane 2, and lane 3, respectively. When the target miRNA was hybridized with the hairpin-locked DNAzyme, the hairpin got unlocked, causing a conformation change in the DNAzyme strand, which made the bands of the DNAzyme/miRNA (lane 4) obviously different from those of the DNAzyme (lane 1). In the absence of the target miRNA and/or Mg^{2+}, the DNAzyme was inactive and could not trigger the cleavage reaction, leaving the substrate bands intact (lanes 5, 6, and 7). Conversely, in the presence of the target miRNA and Mg^{2+}, the DNAzyme hybridized with the target miRNA and then cleaved the substrates, causing the substrate band to disappear (lane 8). The PAGE results confirmed the feasibility of the DNAzyme as an effective signal amplifier.

Optimize the Ratio of DNAzyme and Substrate. For the APCD biosensor, the appropriate ratio of DNAzymes and substrates (D/S) could improve the DNAzyme walking efficiency, thus achieving the maximum amplified fluorescence signal. Based on the different molar ratios of the two components (1:9, 2:8, 3:7, and 4:6), four APCD biosensors were prepared. As shown in Figure S3, fluorescence intensity enhanced with the increase in D/S. When the molar ratio was 2:8, the fluorescence intensity reached the maximum. It indicates that the increase in the DNAzyme proportion contributed to the improvement of walking efficiency, but correspondingly, the decrease in the substrate proportion lead to the signal decrease. Therefore, the optimal molar ratio of D/S 2:8 was used for the subsequent experiments.

Performance of the APCD Biosensors. To explore the quantitative detection performance of the biosensors, we measured the fluorescence intensity in response to the concentrations of miR-135b and miR-133b. As shown in Figure 4a,b, owing to the DNAzyme walking mechanism, the detection signal responded to a dose of each target and increased along with the rising target concentration. Also, the fluorescence intensity of images was getting stronger. The detection results showed that the fluorescence intensity and the concentration of miRNAs (logarithmic scale) exhibited linear relationship from 50 fM to 10 nM (Figure 4c,d). The linear regression equation established according to the concentration−effect relationships was as follows (x-axis, concentration of miRNA; y-axis, FL Intensity)

$y = 9.1328lgx + 56.9568$ ($R^2 = 0.9971$) for detection of the miR-135b concentration.

$y = 11.4405lgx + 69.1081$ ($R^2 = 0.9968$) for detection of the miR-133b concentration.

The LOD as ∼10 fM indicates a higher sensitivity of the biosensors, compared with the other detection methods based on the nanoflare, DNAzyme, or CDs (Table S2). To evaluate the specificity of the APCD biosensor, we mixed the target miRNAs, the point-mutation sequences (1-mut, 3-mut, and 5-mut), and the random miRNA sequence into the APCD biosensor system. As shown in Figure 4e (left), compared with the most significant recovery in the miR-135b group ($P < 0.001$), the signal decreased sharply to 45% (1 mut), 34% (3 mut), 22% (5 mut), and 17% (random). The similar trend of the detection of miR-133b is also showed in Figure 4e (right). The high specificity was mainly attributed to the specific recognition of target sequences by the hairpin-locked-DNAzyme strand. In order to analyze the cross-interference of miR-133b and miR-135b on APCD, the APCD biosensors were incubated with miR-133b, miR-135b, and their mixture, separately. As shown in Figure 4f, fluorescence intensity of the simultaneous detection was consistent with that of the single detection, which indicated that the high specificity and the ideal anti-interference performance enabled the APCD biosensors to detect miRNAs simultaneously.

https://doi.org/10.1021/acs.analchem.1c05588
Anal. Chem. 2022, 94, 4787−4793

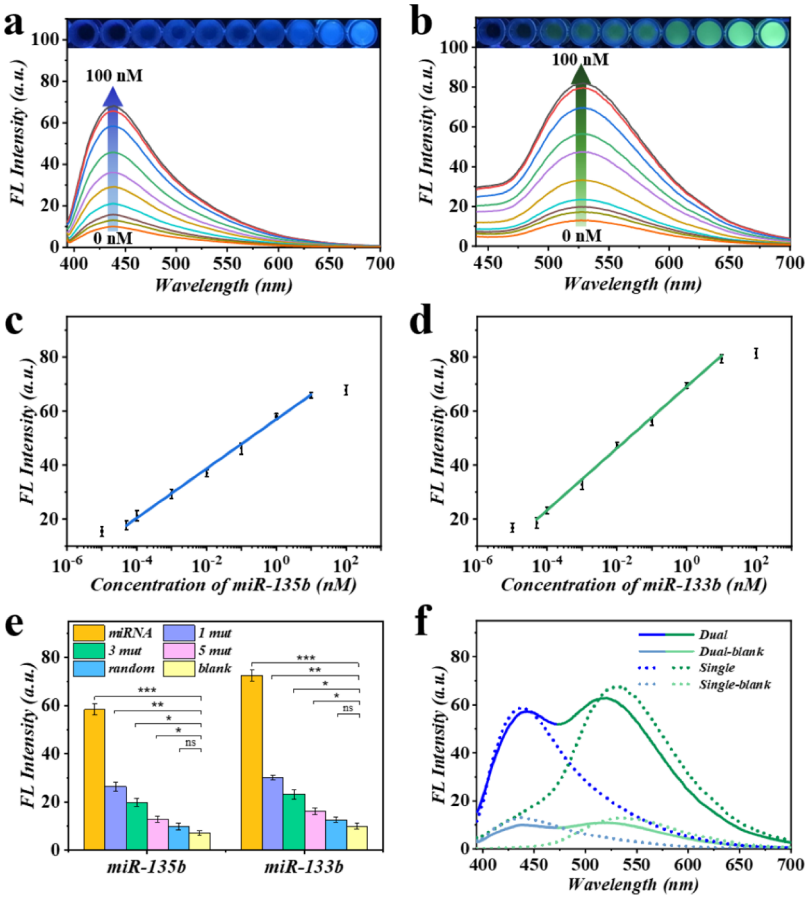

Figure 4. Evaluation of detection performance of the APCD biosensors. Fluorescence detection of target miRNAs based on bCD- (a) and gCD- (b) labeled APCD. The insets show fluorescent images of the APCD biosensors in the presence of different concentrations of the miRNA under the excitation of UV light. Relationships between the fluorescence intensity and miR-135b (c) or miR-133b (d) concentrations. (e) Specificity analysis of the two kinds of APCD biosensors over two target miRNAs and their point-mutation sequences. ***$P < 0.001$, **$P < 0.01$, *$P < 0.05$, ns: no significant difference ($P > 0.05$). (f) Comparison of fluorescence intensity of single- and dual-miRNA detection based on APCD biosensors.

Detection of Clinical Specimen. To demonstrate the applicability of the APCD biosensors in a clinical specimen, we analyzed the response to miR-135b and miR-133b in BC/NC serum exosomes. The concentration of exosomal miRNAs was determined by the fluorescence intensity analysis. As shown in Figure 5, the expression of serum exosomal miR-135b in the BC group was higher than that in the NC group. In contrast, the expression of miR-133b was decreased in BC exosomes. Meanwhile, qRT-PCR was employed to act as references, and the concentration of the target miRNA was calculated according to the standard curves (Figure S4). The measured value of two methods were in good consistence (Figure 5), indicating that our analysis strategy possess high accuracy and applicability.

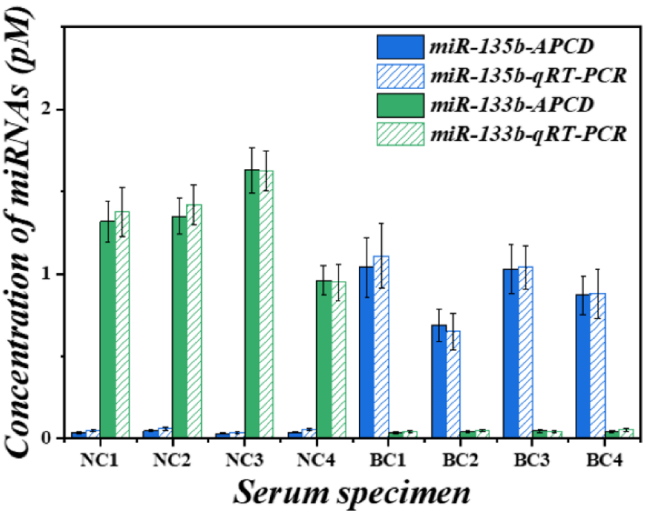

Figure 5. Detection of the exosomal miRNAs extracted from the NC and BC serum by qRT-PCR and the APCD biosensors.

CONCLUSIONS

In summary, the APCD biosensors proposed in this work were synthesized by integrating the AuNP@CDs inorganic nanoflares and DNAzyme walker for simultaneous detection of BC-related exosomal miRNAs. The light-stabilized CDs and the target-specific hairpin-locked DNAzyme enabled the biosensors to achieve the high sensitivity and specificity for miRNA detection. Moreover, simultaneous detection of biomarkers based on the multicolor CDs could further improve the diagnostic efficiency. Notably, the target binding site of the hairpin-locked-DNAzyme strands can be replaced with the complementary sequence of any miRNA, so the APCD biosensors can be used to detect the different miRNAs associated with different diseases. Thus, our strategy has great application potential in cancer diagnosis, including BC.

https://doi.org/10.1021/acs.analchem.1c05588
Anal. Chem. 2022, 94, 4787−4793

■ ASSOCIATED CONTENT

Supporting Information

The Supporting Information is available free of charge at https://pubs.acs.org/doi/10.1021/acs.analchem.1c05588.

Oligonucleotides sequences, mean fold change of miR-135b and miR-133b in BC versus NC serum exosomes, characterization of carbon dots, optimization of the molar ratio of DNAzymes and substrates, and qRT-PCR standard curves (PDF)

■ AUTHOR INFORMATION

Corresponding Authors

Xiaojun Qu − *Laboratory Medicine Center, The Second Affiliated Hospital of Nanjing Medical University, Nanjing 210011, China*; Email: quxiaojun@njmu.edu.cn

Yefei Zhu − *Laboratory Medicine Center, The Second Affiliated Hospital of Nanjing Medical University, Nanjing 210011, China*; orcid.org/0000-0002-2625-2199; Email: zhuyf@njmu.edu.cn

Authors

Xiao Zhang − *Laboratory Medicine Center, The Second Affiliated Hospital of Nanjing Medical University, Nanjing 210011, China*

Xiaowei Wei − *Laboratory Medicine Center, The Second Affiliated Hospital of Nanjing Medical University, Nanjing 210011, China*; orcid.org/0000-0003-2157-505X

Jijin Qi − *Laboratory Medicine Center, The Second Affiliated Hospital of Nanjing Medical University, Nanjing 210011, China*

Jie Shen − *Laboratory Medicine Center, The Second Affiliated Hospital of Nanjing Medical University, Nanjing 210011, China*

Junwen Xu − *Department of Laboratory Medicine, The First People's Hospital of Yancheng, Nanjing University Medical School, Yancheng 224006, China*

Guangyu Gong − *Laboratory Medicine Center, The Second Affiliated Hospital of Nanjing Medical University, Nanjing 210011, China*

Yong Wei − *Department of Urology, The Second Affiliated Hospital of Nanjing Medical University, Nanjing 210011, China*

Jian Yang − *Department of Urology, The Second Affiliated Hospital of Nanjing Medical University, Nanjing 210011, China*

Qingyi Zhu − *Department of Urology, The Second Affiliated Hospital of Nanjing Medical University, Nanjing 210011, China*

Tingting Bai − *Laboratory Medicine Center, The Second Affiliated Hospital of Nanjing Medical University, Nanjing 210011, China*; orcid.org/0000-0002-5849-1469

Zhirui Guo − *Laboratory Medicine Center, The Second Affiliated Hospital of Nanjing Medical University, Nanjing 210011, China*; orcid.org/0000-0003-0332-7159

Complete contact information is available at: https://pubs.acs.org/10.1021/acs.analchem.1c05588

Author Contributions

‖X.Z. and X.W. contributed equally to this paper.

Notes

The authors declare no competing financial interest.

■ ACKNOWLEDGMENTS

This work was supported by the "333 project" High-level Talent Cultivation Foundation of Jiangsu Province, China (Grant number BRA2018086), the Social Development Foundation of the Clinical Frontier Technology of Jiangsu Province, China (grant number BE2017763), and funding support from the Medical Research Project of Jiangsu Province Health Committee, China (grant number K2019020).

■ REFERENCES

(1) Sung, H.; Ferlay, J.; Siegel, R. L.; Laversanne, M.; Soerjomataram, I.; Jemal, A.; Bray, F. *Ca-Cancer J. Clin.* **2021**, *71*, 209−249.

(2) Kaufman, D. S.; Shipley, W. U.; Feldman, A. S. *Lancet* **2009**, *374*, 239−249.

(3) Grayson, M. *Nature* **2017**, *551*, S33.

(4) Xu, R.; Rai, A.; Chen, M.; Suwakulsiri, W.; Greening, D. W.; Simpson, R. J. *Nat. Rev. Clin. Oncol.* **2018**, *15*, 617−638.

(5) Isaac, R.; Reis, F. C. G.; Ying, W.; Olefsky, J. M. *Cell Metab.* **2021**, *33*, 1744−1762.

(6) Cheng, L.; Sharples, R. A.; Scicluna, B. J.; Hill, A. F. *J. Extracell. Vesicles* **2014**, *3*, 23743.

(7) Sun, Z.; Shi, K.; Yang, S.; Liu, J.; Zhou, Q.; Wang, G.; Song, J.; Li, Z.; Zhang, Z.; Yuan, W. *Mol. Cancer* **2018**, *17*, 147.

(8) Jin, X.; Chen, Y.; Chen, H.; Fei, S.; Chen, D.; Cai, X.; Liu, L.; Lin, B.; Su, H.; Zhao, L.; Su, M.; Pan, H.; Shen, L.; Xie, D.; Xie, C. *Clin. Cancer Res.* **2017**, *23*, 5311−5319.

(9) Cho, S.; Yang, H. C.; Rhee, W. J. *Biosens. Bioelectron.* **2019**, *146*, 111749.

(10) Prigodich, A. E.; Seferos, D. S.; Massich, M. D.; Giljohann, D. A.; Lane, B. C.; Mirkin, C. A. *ACS Nano* **2009**, *3*, 2147−2152.

(11) Li, J.; Wang, J.; Liu, S.; Xie, N.; Quan, K.; Yang, Y.; Yang, X.; Huang, J.; Wang, K. *Angew. Chem., Int. Ed. Engl.* **2020**, *59*, 20104−20111.

(12) Liu, L.; Li, N.; Huang, Z.-M.; Tang, L.-J.; Ying, Z.-M.; Jiang, J.-H. *Anal. Chem.* **2020**, *92*, 10925−10929.

(13) Zhao, J.; Liu, C.; Li, Y.; Ma, Y.; Deng, J.; Li, L.; Sun, J. *J. Am. Chem. Soc.* **2020**, *142*, 4996−5001.

(14) Zhai, L.-Y.; Li, M.-X.; Pan, W.-L.; Chen, Y.; Li, M.-M.; Pang, J.-X.; Zheng, L.; Chen, J.-X.; Duan, W.-J. *ACS Appl. Mater. Interfaces* **2018**, *10*, 39478−39486.

(15) Du, J.; Xu, N.; Fan, J.; Sun, W.; Peng, X. *Small* **2019**, *15*, No. e1805087.

(16) Zheng, M.; Ruan, S.; Liu, S.; Sun, T.; Qu, D.; Zhao, H.; Xie, Z.; Gao, H.; Jing, X.; Sun, Z. *ACS Nano* **2015**, *9*, 11455−11461.

(17) Li, L.; Shi, L.; Jia, J.; Eltayeb, O.; Lu, W.; Tang, Y.; Dong, C.; Shuang, S. *ACS Appl. Mater. Interfaces* **2020**, *12*, 18250−18257.

(18) Ji, C.; Zhou, Y.; Leblanc, R. M.; Peng, Z. *ACS Sens.* **2020**, *5*, 2724−2741.

(19) Morrison, D.; Rothenbroker, M.; Li, Y. *Small Methods* **2018**, *2*, 1700319.

(20) Qian, Y.; Wang, C.; Gao, F. *Biosens. Bioelectron.* **2015**, *63*, 425−431.

(21) Peng, H.; Li, X.-F.; Zhang, H.; Le, X. C. *Nat. Commun.* **2017**, *8*, 14378.

(22) Chen, K.; Huang, Q.; Fu, T.; Ke, G.; Zhao, Z.; Zhang, X.; Tan, W. *Anal. Chem.* **2020**, *92*, 7404−7408.

(23) Zhang, H.; Xu, X.; Jiang, W. *Chem. Sci.* **2020**, *11*, 7415−7423.

(24) Qu, S.; Wang, X.; Lu, Q.; Liu, X.; Wang, L. *Angew. Chem., Int. Ed. Engl.* **2012**, *51*, 12215−12218.

(25) Kasprzyk, W.; Świergosz, T.; Bednarz, S.; Walas, K.; Bashmakova, N. V.; Bogdał, D. *Nanoscale* **2018**, *10*, 13889−13894.

(26) Frens, G. *Nature, Phys. Sci.* **1973**, *241*, 20−22.

(27) Hurst, S. J.; Lytton-Jean, A. K. R.; Mirkin, C. A. *Anal. Chem.* **2006**, *78*, 8313−8318.

(28) Cai, X.; Qu, L.; Yang, J.; Xu, J.; Sun, L.; Wei, X.; Qu, X.; Bai, T.; Guo, Z.; Zhu, Y. *Cancer Med.* **2020**, *9*, 6009−6019.

(29) Xu, J.; Wei, X.; Zhang, X.; Cai, Z.; Wei, Y.; Liu, W.; Yang, J.; Li, Y.; Cai, X.; Bai, T.; Guo, Z.; Qu, X.; Zhu, Q.; Zhu, Y. *Sens. Actuators, B* **2021**, *349*, 130824.
(30) Dyrskjøt, L.; Ostenfeld, M. S.; Bramsen, J. B.; Silahtaroglu, A. N.; Lamy, P.; Ramanathan, R.; Fristrup, N.; Jensen, J. L.; Andersen, C. L.; Zieger, K.; Kauppinen, S.; Ulhøi, B. P.; Kjems, J.; Borre, M.; Orntoft, T. F. *Cancer Res.* **2009**, *69*, 4851−4860.

https://doi.org/10.1021/acs.analchem.1c05588
Anal. Chem. 2022, 94, 4787−4793